Title
Status and results from the CUORE experiment

Journal
International Journal of Modern Physics A, 35(36)

ISSN
0217-751X

Authors
Campani, A
Adams, DQ
Alduino, C
et al.

Publication Date
2020-12-30

DOI
10.1142/s0217751x20440169

Peer reviewed

International Journal of Modern Physics A
Vol. 35 (2020) 2044016 (19 pages)

DOI: 10.1142/S0217751X20440169

Status and results from the CUORE experiment

A. Campani*
on behalf of the CUORE Collaboration
Dipartimento di Fisica, Università di Genova, I-16146 Genova, Italy
INFN – Sezione di Genova, I-16146 Genova, Italy
alice.campani@ge.infn.it

D. Q. Adams and C. Alduino
Department of Physics and Astronomy, University of South Carolina, Columbia, SC 29208, USA

K. Alfonso
Department of Physics and Astronomy, University of California, Los Angeles, CA 90095, USA

F. T. Avignone III
Department of Physics and Astronomy, University of South Carolina, Columbia, SC 29208, USA

O. Azzolini
INFN – Laboratori Nazionali di Legnaro, Legnaro (Padova) I-35020, Italy

G. Bari
INFN – Sezione di Bologna, Bologna I-40127, Italy

F. Bellini
Dipartimento di Fisica, Sapienza Università di Roma, Roma I-00185, Italy
INFN – Sezione di Roma, Roma I-00185, Italy

G. Benato
INFN – Laboratori Nazionali del Gran Sasso, Assergi (L'Aquila) I-67100, Italy

M. Biassoni
INFN – Sezione di Milano Bicocca, Milano I-20126, Italy

*Corresponding author.

A. Branca and C. Brofferio

Dipartimento di Fisica, Università di Milano-Bicocca, Milano I-20126, Italy
INFN – Sezione di Milano Bicocca, Milano I-20126, Italy

C. Bucci

INFN – Laboratori Nazionali del Gran Sasso, Assergi (L'Aquila) I-67100, Italy

A. Caminata

INFN – Sezione di Genova, I-16146 Genova, Italy

L. Canonica

Massachusetts Institute of Technology, Cambridge, MA 02139, USA
INFN – Laboratori Nazionali del Gran Sasso, Assergi (L'Aquila) I-67100, Italy

X. G. Cao

Key Laboratory of Nuclear Physics and Ion-Beam Application (MOE),
Institute of Modern Physics, Fudan University, Shanghai 200433, China

S. Capelli

Dipartimento di Fisica, Università di Milano-Bicocca, Milano I-20126, Italy
INFN – Sezione di Milano Bicocca, Milano I-20126, Italy

L. Cappelli

INFN – Laboratori Nazionali del Gran Sasso, Assergi (L'Aquila) I-67100, Italy
Department of Physics, University of California, Berkeley, CA 94720, USA
Nuclear Science Division, Lawrence Berkeley National Laboratory,
Berkeley, CA 94720, USA

L. Cardani

INFN – Sezione di Roma, Roma I-00185, Italy

P. Carniti

Dipartimento di Fisica, Università di Milano-Bicocca, Milano I-20126, Italy
INFN – Sezione di Milano Bicocca, Milano I-20126, Italy

N. Casali

INFN – Sezione di Roma, Roma I-00185, Italy

D. Chiesa

Dipartimento di Fisica, Università di Milano-Bicocca, Milano I-20126, Italy
INFN – Sezione di Milano Bicocca, Milano I-20126, Italy

N. Chott

Department of Physics and Astronomy, University of South Carolina,
Columbia, SC 29208, USA

M. Clemenza

Dipartimento di Fisica, Università di Milano-Bicocca, Milano I-20126, Italy
INFN – Sezione di Milano Bicocca, Milano I-20126, Italy

S. Copello

Dipartimento di Fisica, Università di Genova, I-16146 Genova, Italy
INFN – Sezione di Genova, I-16146 Genova, Italy

C. Cosmelli

Dipartimento di Fisica, Sapienza Università di Roma, Roma I-00185, Italy
INFN – Sezione di Roma, Roma I-00185, Italy

O. Cremonesi

INFN – Sezione di Milano Bicocca, Milano I-20126, Italy

R. J. Creswick

Department of Physics and Astronomy, University of South Carolina, Columbia, SC 29208, USA

A. D'Addabbo[1] and D. D'Aguanno[1,2]

[1]*INFN – Laboratori Nazionali del Gran Sasso, Assergi (L'Aquila) I-67100, Italy*
[2]*Dipartimento di Ingegneria Civile e Meccanica, Università degli Studi di Cassino e del Lazio Meridionale, Cassino I-03043, Italy*

I. Dafinei

INFN – Sezione di Roma, Roma I-00185, Italy

C. J. Davis

Wright Laboratory, Department of Physics, Yale University, New Haven, CT 06520, USA

S. Dell'Oro

Center for Neutrino Physics, Virginia Polytechnic Institute and State University, Blacksburg, Virginia 24061, USA

S. Di Domizio

Dipartimento di Fisica, Università di Genova, I-16146 Genova, Italy
INFN – Sezione di Genova, I-16146 Genova, Italy

V. Dompè

INFN – Laboratori Nazionali del Gran Sasso, Assergi (L'Aquila) I-67100, Italy
INFN – Gran Sasso Science Institute, L'Aquila I-67100, Italy

D. Q. Fang

Key Laboratory of Nuclear Physics and Ion-Beam Application (MOE), Institute of Modern Physics, Fudan University, Shanghai 200433, China

G. Fantini

Dipartimento di Fisica, Sapienza Università di Roma, Roma I-00185, Italy
INFN – Sezione di Roma, Roma I-00185, Italy

M. Faverzani and E. Ferri

Dipartimento di Fisica, Università di Milano-Bicocca, Milano I-20126, Italy
INFN – Sezione di Milano Bicocca, Milano I-20126, Italy

F. Ferroni

INFN – Gran Sasso Science Institute, L'Aquila I-67100, Italy
INFN – Laboratori Nazionali del Gran Sasso, Assergi (L'Aquila) I-67100, Italy

E. Fiorini

INFN – Sezione di Milano Bicocca, Milano I-20126, Italy
Dipartimento di Fisica, Università di Milano-Bicocca, Milano I-20126, Italy

M. A. Franceschi

INFN – Laboratori Nazionali di Frascati, Frascati (Roma) I-00044, Italy

S. J. Freedman[3,4,†] and B. K. Fujikawa[3]

[3]*Nuclear Science Division, Lawrence Berkeley National Laboratory, Berkeley, California 94720, USA*
[4]*Department of Physics, University of California, Berkeley, CA 94720, USA*

A. Giachero and L. Gironi

Dipartimento di Fisica, Università di Milano-Bicocca, Milano I-20126, Italy
INFN – Sezione di Milano Bicocca, Milano I-20126, Italy

A. Giuliani

CSNSM, Univ. Paris-Sud, CNRS/IN2P3, Université Paris-Saclay, 91405 Orsay, France

P. Gorla

INFN – Laboratori Nazionali del Gran Sasso, Assergi (L'Aquila) I-67100, Italy

C. Gotti

Dipartimento di Fisica, Università di Milano-Bicocca, Milano I-20126, Italy
INFN – Sezione di Milano Bicocca, Milano I-20126, Italy

T. D. Gutierrez

Physics Department, California Polytechnic State University, San Luis Obispo, California 93407, USA

K. Han

INPAC and School of Physics and Astronomy, Shanghai Jiao Tong University, Shanghai Laboratory for Particle Physics and Cosmology, Shanghai 200240, China

K. M. Heeger

Wright Laboratory, Department of Physics, Yale University, New Haven, CT 06520, USA

R. G. Huang

Department of Physics, University of California, Berkeley, CA 94720, USA

[†]Deceased

H. Z. Huang

Department of Physics and Astronomy, University of California, Los Angeles, CA 90095, USA

J. Johnston

Massachusetts Institute of Technology, Cambridge, MA 02139, USA

G. Keppel

INFN – Laboratori Nazionali di Legnaro, Legnaro (Padova) I-35020, Italy

Yu. G. Kolomensky

Department of Physics, University of California, Berkeley, CA 94720, USA
Nuclear Science Division, Lawrence Berkeley National Laboratory, Berkeley, California 94720, USA

C. Ligi

INFN – Laboratori Nazionali di Frascati, Frascati (Roma) I-00044, Italy

Y. G. Ma

Key Laboratory of Nuclear Physics and Ion-Beam Application (MOE), Institute of Modern Physics, Fudan University, Shanghai 200433, China

L. Ma

Department of Physics and Astronomy, University of California, Los Angeles, CA 90095, USA

L. Marini

Department of Physics, University of California, Berkeley, CA 94720, USA
Nuclear Science Division, Lawrence Berkeley National Laboratory, Berkeley, California 94720, USA

R. H. Maruyama

Wright Laboratory, Department of Physics, Yale University, New Haven, CT 06520, USA

Y. Mei

Nuclear Science Division, Lawrence Berkeley National Laboratory, Berkeley, California 94720, USA

N. Moggi

Dipartimento di Fisica e Astronomia, Alma Mater Studiorum, Università di Bologna, Bologna I-40127, Italy
INFN – Sezione di Bologna, Bologna I-40127, Italy

S. Morganti

INFN – Sezione di Roma, Roma I-00185, Italy

T. Napolitano
INFN – Laboratori Nazionali di Frascati, Frascati (Roma) I-00044, Italy

M. Nastasi
Dipartimento di Fisica, Università di Milano-Bicocca, Milano I-20126, Italy
INFN – Sezione di Milano Bicocca, Milano I-20126, Italy

J. Nikkel
Wright Laboratory, Department of Physics, Yale University, New Haven, CT 06520, USA

C. Nones
Service de Physique des Particules, CEA/Saclay, 91191 Gif-sur-Yvette, France

E. B. Norman
Lawrence Livermore National Laboratory, Livermore, CA 94550, USA
Department of Nuclear Engineering, University of California, Berkeley, CA 94720, USA

V. Novati
CSNSM, Univ. Paris-Sud, CNRS/IN2P3, Université Paris-Saclay, 91405 Orsay, France

A. Nucciotti and I. Nutini
Dipartimento di Fisica, Università di Milano-Bicocca, Milano I-20126, Italy
INFN – Sezione di Milano Bicocca, Milano I-20126, Italy

T. O'Donnell
Center for Neutrino Physics, Virginia Polytechnic Institute and State University, Blacksburg, Virginia 24061, USA

J. L. Ouellet
Massachusetts Institute of Technology, Cambridge, MA 02139, USA

C. E. Pagliarone
INFN – Laboratori Nazionali del Gran Sasso, Assergi (L'Aquila) I-67100, Italy
Dipartimento di Ingegneria Civile e Meccanica, Università degli Studi di Cassino e del Lazio Meridionale, Cassino I-03043, Italy

L. Pagnanini
Dipartimento di Fisica, Università di Milano-Bicocca, Milano I-20126, Italy
INFN – Sezione di Milano Bicocca, Milano I-20126, Italy

M. Pallavicini
Dipartimento di Fisica, Università di Genova, I-16146 Genova, Italy
INFN – Sezione di Genova, I-16146 Genova, Italy

L. Pattavina

INFN – Laboratori Nazionali del Gran Sasso, Assergi (L'Aquila) I-67100, Italy

M. Pavan

Dipartimento di Fisica, Università di Milano-Bicocca, Milano I-20126, Italy
INFN – Sezione di Milano Bicocca, Milano I-20126, Italy

G. Pessina

INFN – Sezione di Milano Bicocca, Milano I-20126, Italy

V. Pettinacci

INFN – Sezione di Roma, Roma I-00185, Italy

C. Pira

INFN – Laboratori Nazionali di Legnaro, Legnaro (Padova) I-35020, Italy

S. Pirro

INFN – Laboratori Nazionali del Gran Sasso, Assergi (L'Aquila) I-67100, Italy

S. Pozzi

Dipartimento di Fisica, Università di Milano-Bicocca, Milano I-20126, Italy
INFN – Sezione di Milano Bicocca, Milano I-20126, Italy

E. Previtali

INFN – Sezione di Milano Bicocca, Milano I-20126, Italy
Dipartimento di Fisica, Università di Milano-Bicocca, Milano I-20126, Italy

A. Puiu

Dipartimento di Fisica, Università di Milano-Bicocca, Milano I-20126, Italy
INFN – Sezione di Milano Bicocca, Milano I-20126, Italy

C. Rosenfeld

Department of Physics and Astronomy, University of South Carolina, Columbia, South Carolina 29208, USA

C. Rusconi

Department of Physics and Astronomy, University of South Carolina, Columbia, South Carolina 29208, USA
INFN – Laboratori Nazionali del Gran Sasso, Assergi (L'Aquila) I-67100, Italy

M. Sakai

Department of Physics, University of California, Berkeley, CA 94720, USA

S. Sangiorgio

Lawrence Livermore National Laboratory, Livermore, CA 94550, USA

B. Schmidt

Nuclear Science Division, Lawrence Berkeley National Laboratory, Berkeley, California 94720, USA

N. D. Scielzo
Lawrence Livermore National Laboratory, Livermore, CA 94550, USA

V. Sharma
Center for Neutrino Physics, Virginia Polytechnic Institute and State University, Blacksburg, Virginia 24061, USA

V. Singh
Department of Physics, University of California, Berkeley, CA 94720, USA

M. Sisti
Dipartimento di Fisica, Università di Milano-Bicocca, Milano I-20126, Italy
INFN – Sezione di Milano Bicocca, Milano I-20126, Italy

D. Speller and P. T. Surukuchi
Wright Laboratory, Department of Physics, Yale University, New Haven, CT 06520, USA

L. Taffarello
INFN – Sezione di Padova, Padova I-35131, Italy

F. Terranova
Dipartimento di Fisica, Università di Milano-Bicocca, Milano I-20126, Italy
INFN – Sezione di Milano Bicocca, Milano I-20126, Italy

C. Tomei and M. Vignati
INFN – Sezione di Roma, Roma I-00185, Italy

S. L. Wagaarachchi
Department of Physics, University of California, Berkeley, CA 94720, USA
Nuclear Science Division, Lawrence Berkeley National Laboratory, Berkeley, California 94720, USA

B. S. Wang
Lawrence Livermore National Laboratory, Livermore, CA 94550, USA
Department of Nuclear Engineering, University of California, Berkeley, CA 94720, USA

B. Welliver
Nuclear Science Division, Lawrence Berkeley National Laboratory, Berkeley, California 94720, USA

J. Wilson and K. Wilson
Department of Physics and Astronomy, University of South Carolina, Columbia, South Carolina 29208, USA

L. A. Winslow
Massachusetts Institute of Technology, Cambridge, MA 02139, USA

L. Zanotti

Dipartimento di Fisica, Università di Milano-Bicocca, Milano I-20126, Italy
INFN – Sezione di Milano Bicocca, Milano I-20126, Italy

S. Zimmermann

Engineering Division, Lawrence Berkeley National Laboratory, Berkeley, CA 94720, USA

S. Zucchelli

Dipartimento di Fisica e Astronomia, Alma Mater Studiorum, Università di Bologna, Bologna I-40127, Italy
INFN – Sezione di Bologna, Bologna I-40127, Italy

Received 15 June 2020
Accepted 6 November 2020
Published 23 December 2020

The Cryogenic Underground Observatory for Rare Events (CUORE) is a tonne-scale cryogenic experiment located at the Laboratori Nazionali del Gran Sasso that exploits bolometric technique to search for neutrinoless double beta decay ($0\nu\beta\beta$) of ^{130}Te. The detector consists of a segmented array of 988 natural TeO_2 cubic crystals arranged in a cylindrical compact structure of 19 towers. The detector construction was completed in August 2016 and data taking started in Spring 2017. In this work, we present a brief description of the bolometric technique for rare events search and the CUORE detector, then we concentrate on the data analysis results. In this respect, we focus on the procedure for data processing and on the first $0\nu\beta\beta$ results we obtained from a total TeO_2 exposure of 86.3 kg $\cdot$ yr. Next, we illustrate the main background sources and the CUORE background model, from which we obtain the most precise measurement of ^{130}Te $2\nu\beta\beta$ half-life to date. Finally, we discuss the improvements achieved with 2018 and 2019 detector optimization campaigns and the current perspectives of our experiment.

Keywords: Neutrinoless double beta decay; two-neutrino double beta decay; background model.

PACS number: 29.90.+r

1. Introduction

Double beta decay is a rare, second-order nuclear transition in which an initial nucleus (A, Z) decays to a member $(A, Z + 2)$ of the same isobaric multiplet with the simultaneous emission of two electrons and two antineutrinos.[1] Predicted in 1935 by G. Mayer, it is allowed by the Standard Model only for even–even nuclei and it has been observed in many nuclei, such as ^{76}Ge and ^{136}Xe. After the discovery of neutrino flavor oscillations and the conclusion that neutrinos are not massless, the search for the neutrinoless channel of this process became a priority both in nuclear and astroparticle physics. The main feature of $0\nu\beta\beta$ transition is the explicit violation of the lepton number (L) by two units, thus the observation of this decay would unambiguously demonstrate that L is not a symmetry of nature. Even in the absence of direct observation, constraints on the $0\nu\beta\beta$ decay rate can provide

fundamental informations on the neutrino mass scale (*inverted* or *normal* hierarchy) and nature (Dirac or Majorana particles).

In the simplest scheme, $0\nu\beta\beta$ is mediated by the exchange of light neutrinos gifted with Majorana mass. The decay rate can be expressed as

$$\Gamma_{0\nu\beta\beta} = G_{0\nu}|M_{0\nu}|^2 \frac{m_{\beta\beta}^2}{m_e^2}, \quad m_{\beta\beta} = \left| \sum_{i=1,2,3} U_{ei}^2 m_i \right|, \tag{1}$$

where $G_{0\nu}$ is the known space phase factor and $M_{0\nu}$ the nuclear matrix element. $m_{\beta\beta}$ is the effective Majorana mass, that explicitly depends on Majorana phases. In the $2\nu\beta\beta$ mode, the energy spectrum of the final state electrons is a continuum from 0 to the end point (i.e. the Q-value) of the reaction. On the contrary, the experimental signature of the $0\nu\beta\beta$ channel is a monochromatic peak at $Q_{\beta\beta}$.

The experimental sensitivity[a] in $0\nu\beta\beta$ searches is given by $S_{T_{1/2}} \propto \varepsilon \cdot \sqrt{\frac{M \cdot T}{B \cdot \Delta E}}$ where ε is the signal efficiency, M the active mass (kg), T the lifetime (yr), B the background index around $Q_{\beta\beta}$ expressed in counts/(keV $\cdot$ kg $\cdot$ yr) and ΔE the energy resolution at the Q-value. Therefore, to maximize the sensitivity an experiment for $0\nu\beta\beta$ search must have a large source mass, this implies scalability of the experimental technique, a very low background rate near the Q-value and a good energy resolution.

The Cryogenic Underground Observatory for Rare Events (CUORE) is a tonne-scale experiment located at the Laboratori Nazionali del Gran Sasso in Italy. Its main scientific goal is the search for $0\nu\beta\beta$ of ^{130}Te to ^{130}Xe.[2] CUORE has a total active mass of $\sim$742 kg ($\sim$206 kg of ^{130}Te) and its background index goal is 0.01 counts/(keV $\cdot$ kg $\cdot$ yr). CUORE exploits the bolometric technique to reach an energy resolution of $\sim$5 keV FWHM around the Q-value (2525.5 keV). The ultimate CUORE sensitivity to the half-life of ^{130}Te $0\nu\beta\beta$ decay after 5 years of lifetime is $9{\cdot}10^{25}$ yr.[3] The CUORE detector consists of an array of Tellurium dioxide crystals grouped in 19 towers. ^{130}Te has the highest isotopic abundance ($\sim$34.2%) among the nuclei of interest, therefore crystals were made with $^{\text{nat}}$Te. CUORE is located underground as the average LNGS rock overburden of almost 3600 m.w.e. reduces the muon flux by 6 orders of magnitude with respect to sea level.[4] CUORE is operated stably at $\sim$10 mK thanks to a custom-built cryogen free dilution-unit cryostat.

2. The Bolometric Technique and CUORE Detector

The CUORE detector consists of 988 bolometers operating independently, each of them acts as an individual detector searching for ^{130}Te $0\nu\beta\beta$ decay and has a mass of $\sim$750 kg and $5 \times 5 \times 5$ cm^3 size.

A bolometer is a sensitive calorimeter that measures the energy deposited after a particle interaction thanks to the increase in the base temperature of the medium.

[a]If the zero background condition is fulfilled, sensitivity scales linearly with the exposure.

A CUORE bolometer has three primary components:

- an absorber, i.e. the crystal itself;
- a temperature sensor, that converts the temperature rise into a voltage pulse, we use a neutron transmutation doped (NTD) germanium thermistor that is glued to the bolometer surface and has a resistivity exponentially dependent on temperature;
- a link to the copper frame that acts both as structural support and thermal bath to restore the reference temperature.

Each crystal is also equipped with a silicon heater to periodically inject stable voltage pulses with precise and fixed energy in order to monitor and correct for possible variations in the detector temperature and response.

Each thermistor has a typical resistance of $\sim(0.1\text{–}1)$ GΩ and is biased with a constant current. We continuously acquire the voltage at its ends with a sampling frequency of 1 kHz using room temperature electronics. We use the amplitude of NTD pulses to infer the amount energy release in the corresponding crystal.

In order to exploit the heat capacity trend of dielectric materials ($C \propto T^3$, according to Debye law), we must operate the detector at extremely low temperature. CUORE crystals are contained in a powerful custom ^{3}He/^{4}He dilution refrigerator that keeps it in stable conditions at ~ 10 mK.[5] The experimental mass and

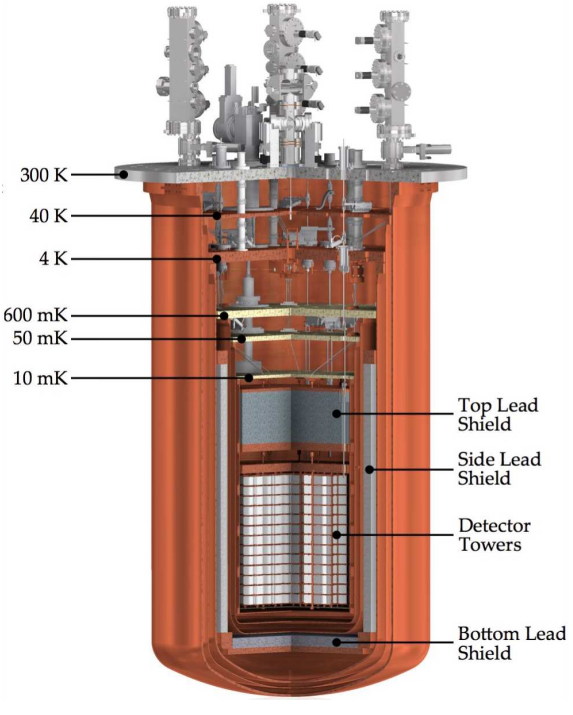

Fig. 1. Rendering of the CUORE cryostat.

volume ($\sim$17 tons and 1 m^3, respectively) make CUORE cryostat the largest and most powerful cryogen free dilution cryostat currently in operation. The operating temperature is a compromise between a maximal thermal gain and an optimized signal bandwidth. At $\sim$10 mK, the typical TeO_2 heat capacity corresponds to a temperature variation $\Delta T \sim 100$ μK per MeV.

As it is schematically shown in Fig. 1, precooling to maintain the dilution cycle is realized by five two-stage ($\sim$40 K and $\sim$4 K) pulse tube cryocoolers, whereas we reach base temperature through the ^{3}He/^{4}He mixture. The cryostat design and construction had to respect very stringent experimental constraints: an effective mechanical insulation, with extremely low vibration levels, and minimal contribution to the radioactive background of the experiment. In particular, in order to suppress the γ and neutron background two lead shields are integrated into the cryogenic volume and a lead + polyethylene shield surrounds the whole cryostat.

A description of the main background sources and an estimate of the background index in the region of interest will be presented in Sec. 4.

3. CUORE Analysis Technique and First $0\nu\beta\beta$ Results

The installation of the CUORE towers inside the cryostat was performed during Summer 2016 and, after the cool-down and an initial detector optimization phase, physics data taking started in Spring 2017.

The data taking is divided in $\sim$ one-month long datasets, each of them is embedded between a few days devoted to the bolometers calibration. We use data collected between calibrations for the $0\nu\beta\beta$ search. In the following, we will refer to them as *physics data*.

Initial calibration has the purpose of identifying the detector response to signals of known energy. The final one is performed to check if the detector response is stable over the whole dataset. During this period, we deploy calibration sources inside the detector. For the analysis presented here, the calibration is based on six γ lines from ^{232}Th. The current calibration system includes also ^{60}Co sources.

A single signal event is contained in a 10-s window: a 3s-pretrigger serves as a measurement of the base temperature, while 7s-pulse gives the amount of energy released in the process. To monitor and model our detector noise behavior we also analyze waveforms that do not contain visible pulses. During the online data acquisition, we save continuous detector waveforms and separately trigger them with a software derivative trigger. Trigger thresholds depend on the noise RMS of single bolometers.

3.1. *The analysis chain*

The CUORE data analysis consists of a series of sequential steps, that we perform using a modular software especially designed for the experiment.

First, we estimate pulse amplitude using an optimum filter that maximizes signal-to-noise ratio. Signal amplitude is then stabilized against thermal drifts using

tagged heater events with fixed energy (see Sec. 2) to avoid spoiling the energy resolution. Additional details on our thermal gain stabilization can be found in Ref. 6. The next step is to identify a calibration function for each bolometer, the best function is a second-order polynomial with zero constant term.

Once the energy of physical events is reconstructed, we discard time periods in which the detector conditions are not optimal (e.g. noisy periods) and apply a series of cut to signals in order to reliably identify $0\nu\beta\beta$ candidate events. Among them, we require the shape of each waveform to be consistent with a true particle-interaction. Thus, we build a signal-like event sample using γ lines from ^{40}K (1461 keV) and ^{60}Co (1173 and 1332 keV, respectively) with six pulse shape parameters and discard all the outlier events.

Since from the CUORE Monte Carlo simulations we expect that the largest fraction of $0\nu\beta\beta$ events ($\sim 88\%$) will release the whole energy in the same crystal in which the decay occurred, we apply an additional anti-coincidence cut to reduce background. Indeed, most of our background events deposit energy across two or more bolometers, e.g. α decays that occur on a surface between neighboring crystals and multiple Compton scatters of γ rays. We assign to each event a value of *multiplicity* (M) to indicate the number of bolometers interested by the same particle process within a certain time window. We optimize it and set a coincidence window of 10 ms (± 5 ms). The analysis threshold for coincident events is set to 150 keV for the analysis presented here. As it will be discussed in Sec. 5, lowering the trigger thresholds thanks to the optimum trigger made it possible to reduce the common analysis threshold to 40 keV.

To avoid a bias in the $0\nu\beta\beta$ decay (fit) result, we blind our data: we move a fraction of events reconstructed at the 2615 keV ^{208}Tl line down by 87 keV to produce an artificial peak at $Q_{\beta\beta}$. As a result, we fix the fit procedure to measure $\Gamma_{0\nu}$ without knowing the real spectrum in the region of interest. This is 110 keV wide and centered at 2527 keV. We evaluate the total signal efficiency as the product of the following components: $0\nu\beta\beta$ containment efficiency, the detection and reconstruction efficiency, the anti-coincidence and the pulse shape analysis efficiency. We use tagged heater pulses to identify trigger and reconstruction efficiency, therefore an estimate for each calorimeter-dataset is provided. On the contrary, anti-coincidence and pulse shape efficiencies are extracted on a dataset basis combining physics data from all the active channels with the procedure outlined in Ref. 6.

We model the CUORE detector response to a monochromatic peak using signals from the high statistics 2615 keV ^{208}Tl γ line in calibration data. The CUORE detectors exhibit a slightly non-Gaussian line shape, as already observed in CUORE-0.[b] We empirically characterize it with a superposition of three Gaussian components, a primary Gaussian peak and two sub-peaks with the same width. We estimate the line shape parameters for each bolometer-dataset performing a

[b]A previous demonstrator for CUORE design and a standalone experiment for $0\nu\beta\beta$ search.

simultaneous unbinned extended maximum likelihood (UELM) fit on each tower. To evaluate possible differences in the detector response between calibration and physics data and account for the energy dependence of the energy resolution, we fit the most prominent peaks in the physics data with the line shape obtained from calibration. We use the fit results to extract an estimate of the energy calibration bias (i.e. the difference between the expected and reconstructed energy of a peak) and the energy resolution scaling, then we compute them at $Q_{\beta\beta}$. Finally, we perform the ROI fit for the $0\nu\beta\beta$ search including three components: a flat background, a signal peak and a peak for the ^{60}Co coincident γ rays at 2505.7 keV. We model both the $0\nu\beta\beta$ and the ^{60}Co sum peak with the three Gaussian line shape previously described.

3.2. *The first results*

The first result on $0\nu\beta\beta$ of ^{130}Te was obtained with two datasets acquired in 2017. A total of 984 over 988 channels is active and the overall average event rate is $\sim$50 mHz in calibration and $\sim$6 mHz in physics data. The total TeO_2 exposure is 86.4 kg$\cdot$yr (^{130}Te 24.0 kg$\cdot$yr). The bolometers have trigger threshold ranging from 20 keV to a few hundred keV. The energetic resolution (FWHM) is (8.3 ± 0.4) keV for the first dataset and (7.4 ± 0.7) keV for the second one.

Figure 2 shows the 155 candidate events in the ROI with the result of the UELM fit superimposed.

The observed background index is (0.014 ± 0.002) counts/(keV$\cdot$kg$\cdot$yr) in line with our expectations. The best fit $\Gamma_{0\nu\beta\beta}$ is $\left(-1.0^{+0.4}_{-0.3}\,(\text{stat.}) \pm 0.1\,(\text{syst.})\right)$ 10^{-25} yr^{-1}. We conclude that there is no evidence for $0\nu\beta\beta$ decay and set a

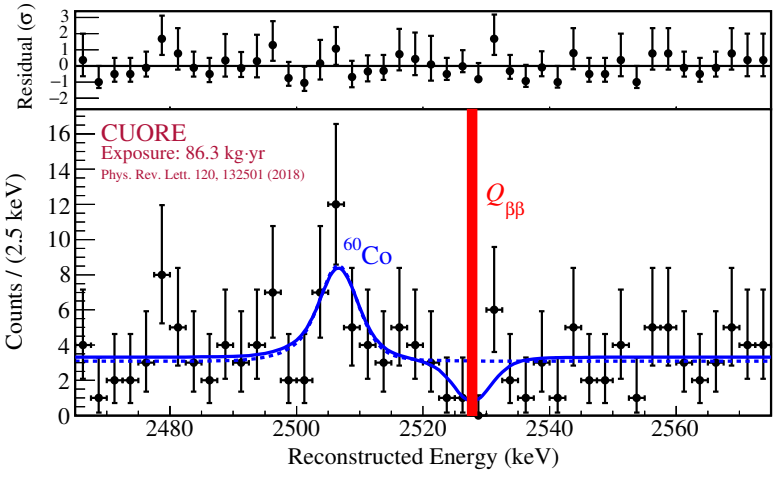

Fig. 2. (Color online) Bottom: best fit model (solid blue line) overlaid on the spectrum of $0\nu\beta\beta$ decay candidates. The vertical band is centered at $Q_{\beta\beta}$. Top: normalized residuals (picture taken from Ref. 6).

90% confidence Bayesian upper limit on the ^{130}Te half-life $T^{0\nu}_{1/2} > 1.3 \cdot 10^{25}$ yr. Combining this result with the limits obtained by CUORE predecessor experiments, Cuoricino and CUORE-0, the limit on $0\nu\beta\beta$ half-life of ^{130}Te becomes $T^{0\nu}_{1/2} > 1.5 \cdot 10^{25}$ yr (90% C.L.). In the framework of $0\nu\beta\beta$ mediated by light Majorana neutrino exchange, we interpret this result as a limit on the effective Majorana mass: $m_{\beta\beta} < (140 - 400)$ meV.[6]

4. CUORE Background Model and Measurement of ^{130}Te $2\nu\beta\beta$ Half-life

As it was mentioned in Sec. 1, the CUORE goal is a 90% C.L. exclusion sensivity of $9 \cdot 10^{-25}$ yr on the $0\nu\beta\beta$ ^{130}Te half-life with 5 years lifetime. This result drove most of the strategies adopted for the realization of CUORE including the strict material selection and the design of highly efficient shielding from radioactivity.

To identify the main background sources in the physics spectrum, we exploited the materials radio assay campaign performed during detector construction and the analysis of CUORE-0 data. CUORE-0 is a prototype of the CUORE detector made of a single tower. It was designed to be a full scale test of the new surface cleaning and detector assembly protocols developed to reduce the α background in the CUORE spectrum.

The most common background sources for underground experiments are long-lived radioactive nuclei as ^{40}K, ^{232}Th and ^{238}U, the latter being progenitors of decay chains. The cosmogenic activation, caused mainly by fast nucleon interactions in copper (detector holder structure) and tellurium (crystals), resulting in ^{60}Co is also a primary component. Finally, a small contribution from cosmic muons, environmental gamma rays and neutrons interacting directly in the detector is also present.

Surface contaminations of the crystals and the materials directly surrounding them represent the major contribution in the region of interest for $0\nu\beta\beta$ decay search. The final estimate of the background index in the region of interest is $(1.02 \pm 0.03\,(\text{stat.})^{+0.23}_{-0.10}\,(\text{syst.}))\ 10^{-2}$ count/keV/kg/yr.[4]

A detailed Geant4-based Monte Carlo simulation of the CUORE experiment has been developed to study the effect of various background sources on CUORE spectrum.

The detector elements included in the model are the following: the crystals, the copper structure holding the towers, the copper vessel enclosing the detector, the Roman lead, both the internal and the external lead shields and the cryostat thermal shields. They account for surface contaminations (near detector elements) and bulk contaminations (near and far detector elements). Their contributions are split in 60 parameters. An additional component to account for the cosmogenic muon flux is included, the total number of simulations is therefore 61.

The simulation code generates and propagates primary and secondary particles through the CUORE geometry until they are detected in the crystals. The output contains the energy and time of all the energy depositions. A second program applies

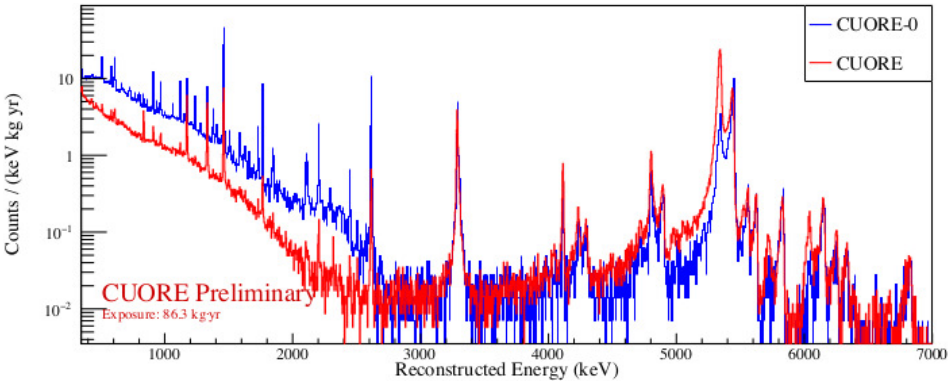

Fig. 3. (Color online) The observed CUORE M1 spectrum (red) versus the CUORE-0 M1 spectrum (blue). We see a significant decrease in the counting rate in the γ-region (below 3 MeV) and an overall consistency with expectations in the α region. An excess of ^{210}Po surface events is visible as the larger peak near 5.3 MeV. However, the good agreement around 3 MeV hints that the increase in the ROI background should be negligible (picture taken from Ref. 8).

a detector response function and incorporates other read-out features: both physical processes and instrumental effects are included. MC implementation is outlined in Ref. 7.

To quantify and disentangle the main background sources, we refer to the same set of data used for the $0\nu\beta\beta$ decay search. The total exposure is 86.3 kg $\cdot$ yr.

The summed spectrum compared with the total spectrum of CUORE-0 is reported in Fig. 3. Overall, CUORE data are consistent with the expectations: the significant decrease in the γ background (below $\sim$3 MeV) is mainly due to the improvements in the material selection and shielding of the cryostat elements, but also the detector self-shielding thanks to its larger volume-to-surface ratio plays an important role. Most of the α region is consistent with what we observed in CUORE-0 as the same assembly procedure and surface cleaning was followed in building the crystals. The only unexpected feature is the excess of surface ^{210}Po events near 5.4 MeV. Its source is still unexplained, but it appears to come from shallow contaminations (from $\sim$0.01 μm to 1 μm) in the copper surrounding the bolometers. Fortunately, its contribution to the ROI background appears to be negligible, i.e. $\sim 10^{-4}$ counts/keV/kg/yr near $Q_{\beta\beta}$.

To understand the observed spectrum, we exploit the main parameters of the event, such as energy, time and the triggering bolometer, but also the *topology* of the event: the analysis of coincidences (see Subsec. 3.1) allows to group events that occurred in a 10 ms window into multiplets. Given the low trigger rate ($\sim$6 mHz), the probability of accidental coincidences is extremely small ($\sim 10^{-5}$) and the majority of multiplets correspond to true physical coincidences. We split data into three types of spectra:

- a multiplicity 1 (M_1) spectrum of the events where all the energy was released in a single crystal;

- a multiplicity 2 (M_2) spectrum including the single bolometer energies of the events satisfying the requirement that two bolometers triggered;
- an M_2 sum spectrum (Σ_2) including an entry with energy equal to the sum of single bolometer energies for each M_2 multiplet.

Double beta decay events are usually confined within the crystal they originated from. Thus, we expect them to end up primarily in the M_1 spectrum. On the contrary, scatterings of γ rays and α decays from contaminants on the surface between two neighboring crystals, deposit energy across two or more bolometers within the response time of the detector. This makes M_2 and Σ_2 spectra fundamental to understand the CUORE background. Due to low statistics, higher multiplicity spectra are a negligible contribution. Therefore, we use them only to evaluate the contribution of muons to the background.

As we expect inner core bolometers to be more shielded from external background, we additionally split M_1 spectrum in two independent spectra. The *outer* layer (M_1^{ext}) includes 736 crystals belonging to the outer (12) towers and the first/last floor of the internal ones. The *inner* layer (M_1^{int}) is made of the 252 remaining crystals.

We reconstruct the background by fitting the simulated spectra to the observed data simultaneously across the four spectra described: M_1^{int}, M_1^{ext}, M_2 and Σ_2. Both the observed and MC spectra are binned with variable bin size to reduce the effect of complicated line shapes. The fit is performed in a Bayesian approach, using a Markov chain Monte Carlo implemented in the JAGS (*Just Another Gibbs Sampler*) software package.[7] For each source a prior probability distribution is defined according to the knowledge already available on its activity.

The measured spectrum from the inner layer crystals and its JAGS reconstruction are reported in Fig. 4. Overall, the model is able to reproduce the major

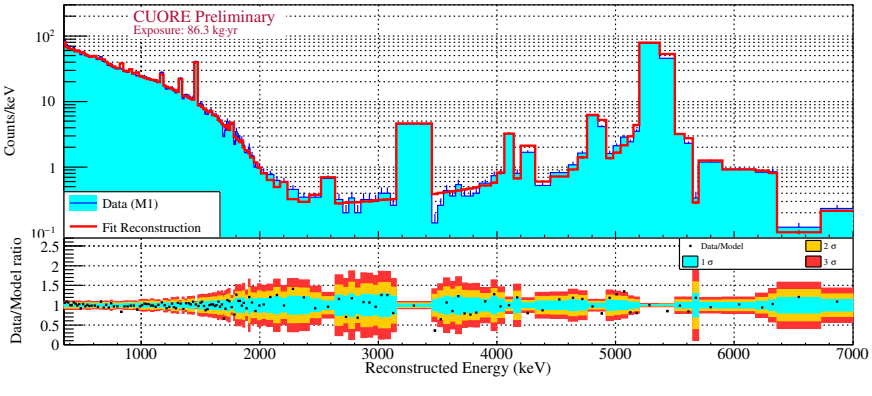

Fig. 4. (Color online) Top: The measured M_1^{int} spectrum (blue) and its MC reconstruction (*red*). An adaptive binning is applied to both histograms to avoid peak shape dependent effects. Bottom: The ratio of the data to the reconstructed model with 1σ, 2σ and 3σ error bars (picture taken from Ref. 8).

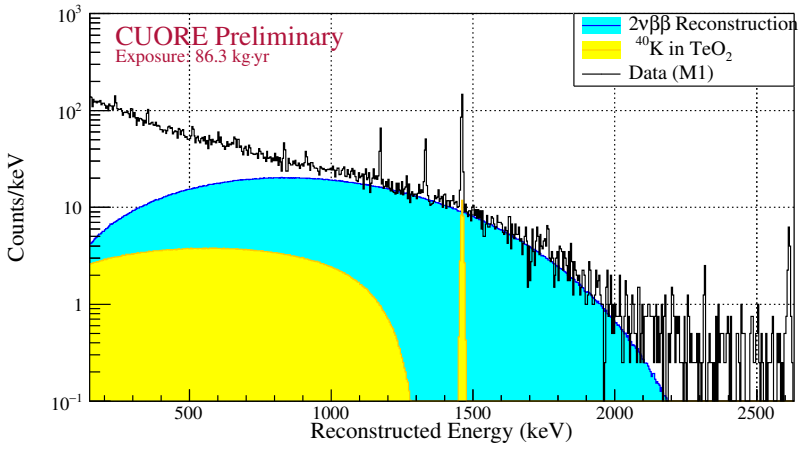

Fig. 5. (Color online) The observed M_1^{int} spectrum (*black*) with a reconstruction of the $2\nu\beta\beta$ background component (*blue*) as well as ^{40}K (*yellow*) (picture taken from Ref. 8).

features of the observed spectra. Much of the disagreement is caused by a poor reconstruction in the α region. This indicates that we have not properly modeled all the background sources leading to these events and we need to refine our description of the detector response to α particles coming from surface contaminants. In order to check the stability of the background model, the dependence on priors and systematic uncertainties, we run a number of different fits varying the binning, the energy threshold, depth of surface contaminations, list of background sources and input data. We find that the leading effect is the geometric splitting of data into subgroups: the uncertainty arising from other terms is about one order of magnitude lower. Despite systematic uncertainties, we were able to extract a robust estimate of the ^{130}Te $2\nu\beta\beta$ half-life. Given the very low γ-background and increased ^{130}Te mass of CUORE, this is the dominant component of the observed M_1 spectrum from $\sim$1–2 MeV as shown in Fig. 5. To prevent bias while tuning data quality cuts and defining the fit procedure, we blinded our MC normalization constant. Once the fit procedure was fixed, we unblinded the normalization factor and extracted a measurement of ^{130}Te $2\nu\beta\beta$ half-life. $T^{2\nu}_{1/2} = [7.9 \pm 0.1\,(\text{stat.}) \pm 0.2\,(\text{syst.})] \cdot 10^{20}$ yr[8] is the most precise measurement to date and is consistent with previous measurements from CUORE-0[7] and NEMO-3.[9]

As a final remark, we mention that the source most correlated to the $2\nu\beta\beta$ decay rate is the ^{40}K in the bulk of the bolometers. A similar effect was observed in CUORE-0, but the larger statistics of CUORE and the lower background makes this a small ($\sim$1%) source of uncertainty on the final measured rate.

5. CUORE Perspectives

CUORE started data taking in Spring 2017. It was the first time such a large number of bolometers were simultaneously operated in a complex cryogenic apparatus.

Therefore, dedicate detector characterization and optimization campaigns were required in these years. Besides various activities related to cryostat maintenance, in 2018 we made a scan of the detector performance as a function of temperature to identify the minimal noise condition. This led us to switch the working temperature from 15 mK to 11 mK.

Data taking is ongoing in stable working conditions since march 2019 and an improved result on ^{130}Te $0\nu\beta\beta$ half-life with an exposure ~ 4 times the one presented here has been submitted to *Physical Review Letters* for publication.[10] This search benefits from lower trigger thresholds and improvements in our analysis software, e.g. in the reconstruction of coincidences. The main difference with respect to the first data release is represented by the trigger algorithm: all CUORE datasets were retriggered offline using a trigger algorithm based on the optimum filter that optimizes the signal-to-noise ratio and significantly reduces trigger thresholds to few times the baseline RMS. Thus, we could lower the common analysis threshold from 150 keV to 40 keV and have access to the low energy region (below ~ 200 keV) of the spectrum. As a consequence, an improvement in our background model reconstruction, especially the estimate of the contribution in the α region due to surface contaminations, is also foreseen.

In conclusion, after a period of upgrades and optimization, CUORE has entered a period of stable data taking thus proving the scalability of the bolometric technique for rare events search. We continue to work to improve our comprehension of the detector response in order to reach our energy resolution goal of 5 keV FWHM and a ROI background index of 0.01 counts/keV/kg/yr.

References

1. W. H. Furry, *Phys. Rev.* **56**, 1184 (1939).
2. CUORE Collab. (D. R. Artusa *et al.*), *Adv. High Energy Phys.* **2015**, 879871 (2015).
3. CUORE Collab. (C. Alduino *et al.*), *Eur. Phys. J. C* **77**, 532 (2017).
4. CUORE Collab. (C. Alduino *et al.*), *Eur. Phys. J. C* **77**, 543 (2017).
5. CUORE Collab. (A. D'Addabbo *et al.*), *J. Low. Temp. Phys.* **193**, 867 (2018).
6. CUORE Collab. (C. Alduino *et al.*), *Phys. Rev. Lett.* **120**, 132501 (2018).
7. CUORE Collab. (C. Alduino *et al.*), *Eur. Phys. J. C* **77**, 13 (2017).
8. CUORE Collab. (D. Q. Adams *et al.*), arXiv:1808.10342 [nucl-ex].
9. NEMO-3 Collab. (R. Arnold *et al.*), *Phys. Rev. Lett.* **107**, 062504 (2011).
10. CUORE Collab. (D. Q. Adams *et al.*), *Phys. Rev. Lett.* **124**, 22501 (2020).